Structure and Dynamics of an Acid-Denatured Protein G Mutant†

Nese Sari, Patrick Alexander, Philip N. Bryan, and John Orban*

Center for Advanced Research in Biotechnology, University of Maryland Biotechnology Institute, 9600 Gudelsky Drive, Rockville, Maryland 20850

Received August 30, 1999; Revised Manuscript Received October 19, 1999

ABSTRACT: NMR studies of protein denatured states provide insights into potential initiation sites for folding that may be too transient to be observed kinetically. We have characterized the structure and dynamics of the acid-denatured state of protein G by using a F30H mutant of G_{B1} which is on the margin of stability. At 5 °C, F30H-G_{B1} is greater than 95% folded at pH 7.0 and is greater than 95% unfolded at pH 4.0. This range of stability is useful because the denatured state can be examined under relatively mild conditions which are optimal for folding G_{B1}. We have assigned almost all backbone ^{15}N, H_N, and H_α resonances in the acid-denatured state. Chemical shift, coupling constant, and NOE data indicate that the denatured state has considerably more residual structure when studied under these mild conditions than in the presence of chemical denaturants. The acid-denatured state populates nativelike conformations with both α-helical and β-hairpin characteristics. To our knowledge, this is the first example of a denatured state with NOE and coupling constant evidence for β-hairpin character. A number of non-native turn structures are also detected, particularly in the region corresponding to the β1−β2 hairpin of the folded state. Steady-state {$^1H-^{15}N$} NOE results demonstrate restricted backbone flexibility in more structured regions of the denatured protein. Overall, our studies suggest that regions of the helix, the β3−β4 hairpin, and the β1−β2 turn may serve as potential initiation sites for folding of G_B. Furthermore, residual structure in acid-denatured F30H-G_{B1} is more extensive than in peptide fragments corresponding to the β1−β2, α-helix, and β3−β4 regions, suggesting additional medium-to-long-range interactions in the full-length polypeptide chain.

Protein G is a multidomain component of the cell wall of streptococcal species from the Lancefield group G and binds to all subclasses of human IgG by the constant Fc region (*1*−*3*). Depending on the strain, protein G contains two or three IgG-binding domains, denoted here as G_B. Several protein G genes have been cloned and sequenced (*4*, *5*). Protein G is organized into functional domains similar to staphylococcal protein A (*6*), and the IgG-binding domains are similar in size. These G_B domains consist of 56 amino acids and are independent folding units that have been characterized structurally using both NMR (*7*−*9*) and X-ray crystallographic methods (*10*−*12*).

The G_B domain has been used as a prototypical model system for the study of protein folding and stability (*13*−*22*). It is on the lower limit in size for a stable unique protein structure and achieves its stability without disulfide bonds or tight ligand binding. The thermodynamic parameters for the unfolding reaction have been determined calorimetrically (*13*) and also from hydrogen exchange measurements (*15*, *17*). In the most general features, the energetics of folding are similar to globular proteins of much larger size. The kinetics of folding and unfolding for two G_B domains, G_{B1} and G_{B2}, have been measured using stopped-flow mixing methods and analyzed according to transition state theory (*14*). G_B contains no prolines, and the kinetics of folding and unfolding fit to a single, first-order rate constant over the temperature range of 5−35 °C with rates of around 200 s^{-1} at pH 7. Pulse-labeling experiments are consistent with these studies and show that the polypeptide chain folds rapidly with a half-life of 5 ms (*16*).

When folding is this fast it is very difficult to obtain a picture of the order in which events take place on the folding pathway(s). Peptide fragments can be synthesized, and this provides a useful way of understanding which secondary structural motifs are the most stable (e.g., see refs *23*−*27*). An obvious limitation here is that any long-range interactions that may be important in stabilizing transient intermediates in the folding process will not be detected. Another approach is to look for residual structure in the denatured states of proteins using multidimensional NMR spectroscopy. Identification of such residual structure, defined as any deviation from random coil (ϕ,ψ)-space, may provide insights into potential initiation sites for folding that may be too transient to be observed kinetically. These types of studies have the added advantage that the full polypeptide chain is used for the structural analysis. This strategy has been used effectively for structural characterization of a number of protein denatured states including the 434 repressor (*28*), barnase (*29*−*31*), staphylococcal nuclease (*32*, *33*), the FK506 binding protein (*34*), drkN SH3 domain (*35*−*37*), barstar (*38*), an immunoglobulin superfamily domain (*39*), and apomyoglobin (*40*). It is important to emphasize here that these studies do not determine unique or stable structures

† Supported by NSF Grant MCB-92-19309, NIST Grant COMM 60NANB6D0108, and NIH Grant GM42560.

* To whom correspondence should be addressed. Phone: 301-738-6221; FAX: 301-738-6255; E-mail: john@magpie.carb.nist.gov.

10.1021/bi9920230 CCC: $19.00
Published on Web 01/12/2000

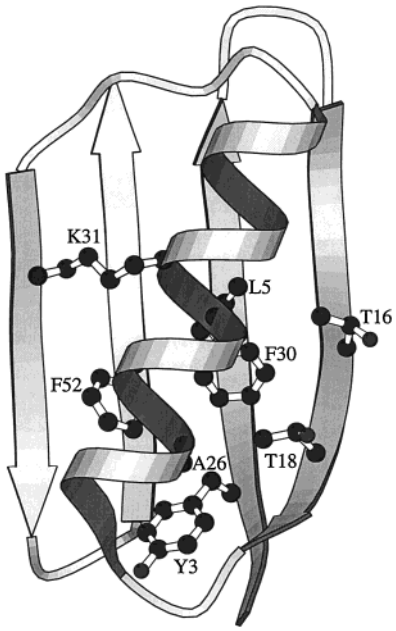

FIGURE 1: X-ray structure of wild-type G_{B1} (*11*) showing the positions of F30 and neighboring residues. MOLSCRIPT (*87*) was used to generate the figure.

but rather any conformational preferences within the ensemble that comprises the "unfolded state".

One problem with this approach is choosing a suitable way of denaturing the protein in question. Recent studies comparing different methods of denaturation in the SH3 domain (*35*, *36*) and barnase (*30*) showed that denatured states studied under relatively mild conditions using changes in pH or ionic strength have considerably more residual structure than denatured states generated with chaotropic agents such as urea or guanidine hydrochloride. Therefore, with regard to these types of NMR studies, there are distinct advantages to studying denatured states under conditions that favor folding (at least weakly), and these will probably also be more biologically relevant.

Since wild-type G_{B1} is stable over a wide range of solution conditions from pH 2 to pH 10 (*13*, *19*), there appear to be no simple alternatives to the use of chemical denaturants. A previous study on the denatured state of G_{B1} in 7.4 M urea at pH 2 indicated that the protein is essentially random coil under these conditions (*41*). Our approach has been to design a mutant of G_{B1} which is on the margin of stability. Mutation of F30, which is buried in the hydrophobic core of the protein (Figure 1), to a histidine provides a simple proton-linked switch for reversible folding and unfolding under relatively mild conditions. At 5 °C, F30H-G_{B1} is greater than 95% folded at pH 7.0 and is greater than 95% unfolded at pH 4.0. This paper describes structural and dynamic characterization of the acid-denatured state of F30H-G_{B1} using NMR spectroscopy. We show that this denatured state contains a significant population of nativelike structure with both α-helical and β-hairpin characteristics. To our knowledge, this is the first example of a denatured state with NOE and coupling constant evidence for β-hairpin character. We also observe non-native NOEs consistent with helix or turn structures in a region corresponding to a β-strand in the native state. This result is similar to recent findings for the drkN SH3 domain denatured under mild conditions (*35*−*37*). Overall, our structural studies suggest that the $\beta1-\beta2$ turn, regions of the α-helix, and the $\beta3-\beta4$ hairpin may serve as potential initiation sites for folding in protein G. These results are complemented by steady-state $\{^1H-^{15}N\}$ NOE measurements that indicate restricted motions on the picosecond to nanosecond time scale in these regions. In addition, our results are compared with findings from peptide fragment and computational studies on the folding of protein G.

MATERIALS AND METHODS

Cloning and Expression. Uracil containing single-stranded DNA was obtained by superinfecting *E. coli* RZ1032 harboring pG7 (*13*) with M13K07 using the method of Kunkel (*42*). Site-directed mutagenesis was performed using standard molecular biology techniques. Mutations were confirmed by sequencing of inserts according to the Sequenase protocol (U. S. Biochemical). Expression, ^{15}N-labeling, and purification were as described previously (*13*, *17*). Samples were stored at 3.8 mg/mL in 10% glycerol in 50 mM potassium phosphate buffer (pH 7.5) at −20 °C.

Kinetic Analysis. Folding kinetics were measured using a KinTek Stopped-Flow model SF2001 (excitation $\lambda = 295$ nm, emission = 340 nm cutoff filter). F30H-G_{B1} was denatured by dissolving lyophilized protein in 0.1 M H_3PO_4. The sample was neutralized by mixing the protein/H_3PO_4 solution into an equal volume of 0.2 M potassium phosphate, pH 11.9, in the KinTek Stopped-Flow (final buffer concentrations were 0.15 M KP_i, pH 7.6). The final concentration of F30H-G_{B1} was 2 μM. Ten kinetics traces were collected and averaged.

Circular Dichroism. Circular dichroism (CD) measurements were performed with a Jasco spectropolarimeter, model J-720, using water-jacketed quartz cells with path lengths of 1 cm, 1 mm, or 0.1 mm depending on F30H-G_{B1} concentrations which ranged from 5 to 800 μM. Temperature control was provided by a Neslab RTE-110 circulating water bath interfaced with a MTP-6 temperature programmer. Far-UV wavelength scans were recorded at 25 °C from 250 to 190 nm. Typically, the average for five CD spectra is presented. The ellipticity results were expressed as mean residue ellipticity (MRE) in units of deg cm^2 dmol^{-1}.

Temperature-induced unfolding of F30H-G_{B1} was performed in the temperature range between 0 and 60 °C in a 0.01 cm cuvette. Ellipticities at 222 nm were continuously monitored at a scanning rate of 1 °C/min. Reversibility of the denaturations was confirmed by comparing the CD spectra at 25 °C before and after cooling or heating. The reversibility was about 80%.

Steady-state fluorescence measurements were made using a SPEX FluoroMax spectrofluorimeter.

NMR Sample Preparation. NMR samples were prepared by concentrating the stock solution to either 0.5 mM or 2.2 mM F30H-G_{B1} in 50 mM potassium phosphate buffer, pH 7.0, using a Centricon 3 kDa cutoff filter (Amicon). Care was taken to ensure complete removal of glycerol, and samples contained 10% D_2O/90% H_2O. The pH was then adjusted to either 7.4, 5.5, or 3.5 with a Sentron microelectrode using sodium hydroxide or HCl solutions. The final sample volume for NMR analysis was 0.45 mL. For titrations, the sample was prepared similarly and the pH was adjusted from 7.3 to 2.2.

NMR Spectroscopy. NMR spectra were recorded on Bruker DRX-500 and DRX-600 spectrometers equipped with 3-axis

gradient probes. Data were processed on Silicon Graphics work stations using Azara (W. Boucher, unpublished results) or NMRPipe (*43*). Two-dimensional homonuclear TOCSY (*44*) and NOESY (*45*) experiments were recorded at 5 and 25 °C using a WATERGATE solvent suppression scheme (*46*) with a spectral width of 6024 Hz (at 500 MHz), 4K complex points, and a relaxation delay of 1−2 s. Mixing times for the TOCSY and NOESY were 55 and 150 ms, respectively. Two-dimensional ^{1}H−^{15}N HSQC spectra were recorded in States-TPPI mode using a gradient water flip-back scheme for solvent suppression (*47*). ^{15}N-Decoupling during t_2 was achieved using a GARP sequence (*48*) with spectral widths in the ^{1}H and ^{15}N dimensions of 7788 and 2032 Hz, respectively, at 600 MHz. HSQC spectra typically consisted of 256 t_1 increments of 1K complex points with 8 scans per increment.

Three-dimensional ^{15}N NOESY−HSQC and ^{15}N TOCSY−HSQC (*49*) experiments were recorded at 600 MHz with mixing times of 100 and 250 ms (NOESY) and 55 ms (TOCSY), at 5 and 25 °C. For the ^{15}N NOESY−HSQC experiment, 76 t_1, 35 t_2, and 512 t_3 complex points were utilized with spectral widths of 7862, 2007, and 7862 Hz (F_1, F_2, F_3). For the ^{15}N TOCSY−HSQC experiment, 60 × 20 × 512 complex points were collected in the $t_1 \times t_2 \times t_3$ dimensions with spectral widths of 7788, 2007, and 7788 Hz (F_1, F_2, F_3) utilizing the DIPSI-2 mixing sequence (*50, 51*). In addition, 3D ^{15}N HMQC−NOESY−HSQC spectra (*52*) were acquired with a 250 ms mixing time and 40 × 40 × 512 complex points in $t_1 \times t_2 \times t_3$ using the spectral widths of 2007, 2007 and 7862 Hz in F_1, F_2, and F_3, respectively. The 3D HNHA experiment (*53, 54*) was recorded as 67 × 32 × 512 complex points in $t_1 \times t_2 \times t_3$ dimensions with spectral widths of 7801, 3049, and 7788 Hz (F_1, F_2, F_3) at 5 °C, 600 MHz. In all 3D experiments, a relaxation delay of 1 s was used with 16 or 32 transients per increment, and ^{15}N-decoupling during acquisition was achieved using a WALTZ-16 sequence (*55*).

The steady-state {^{1}H−^{15}N} NOEs were measured using ^{1}H−^{15}N correlation spectra with a gradient-selected, sensitivity-enhanced pulse sequence as described by Farrow et al. (*56*). A relaxation delay of 2 s prior to a 3 s proton presaturation period was employed for the experiments with NOE, and presaturation was applied 4 MHz off-resonance with the same recycling delay (5 s) for the experiments without NOE. NOE measurements were done the same way at 0, 5, 10, 15, 25, and 40 °C at 500 MHz with the exception of a 4 s relaxation delay prior to a 3 s proton presaturation period at 40 °C. For all the {^{1}H−^{15}N} NOE experiments, the spectral widths were 6010 and 1673 Hz in F_2 and F_1, respectively. NOE experiments were collected as 128 × 1024 complex point data sets with 16 scans per t_1 point, and a WALTZ-16 sequence was used for ^{15}N-decoupling during t_2. The NOEs were calculated from the ratios of the peak heights in the spectrum recorded with proton saturation to the peak heights in the spectrum recorded without saturation.

RESULTS

Reversible Acid Denaturation of F30H-G_{B1}. Circular dichroic spectra in the far-UV region were used to determine the apparent equilibrium constant for folding of F30H-G_{B1} as a function of pH and temperature. Figure 2A shows the CD spectra of wild-type G_{B1}, F30H-G_{B1} in 0.1 M potassium phosphate pH 7.2 at 25 °C, and F30H-G_{B1} in 0.1 M sodium acetate, pH 3.8 at 25 °C. F30H-G_{B1} appears from CD to be 75% folded at 25 °C. At pH 3.8 and 25 °C, the CD spectrum of F30H-G_{B1} is similar to that expected of a largely random coil structure with a minimum ellipticity at 200 nm.

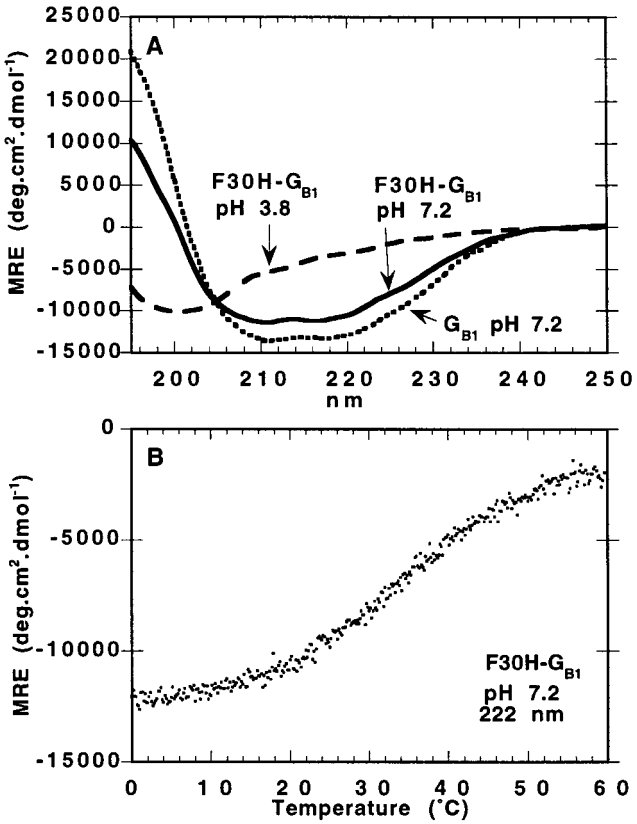

FIGURE 2: (A) CD spectra of F30H-G_{B1} at pH 7.2 (folded, solid line) and pH 3.8 (unfolded, dashed line). The spectrum of wild-type G_{B1} at pH 7.2 (dotted line) is included for comparison purposes. (B) Thermal melt for F30H-G_{B1} at pH 7.2 obtained by monitoring the ellipticity at 222 nm as a function of temperature.

The temperature unfolding profile of F30H-G_{B1} at pH 7.2, as monitored at 222 nm, is presented in Figure 2B. F30H-G_{B1} appears to be greater than 95% folded at 5 °C based on comparison with the CD spectrum of G_{B1} (Figure 2A). The midpoint of the thermal transition occurs around 35 °C. Therefore, mutation at this position decreases the thermal stability of the protein significantly from wild-type G_{B1} where the T_m is 88 °C under similar conditions (*13*).

The pH-dependent stability of F30H-G_{B1} was also characterized at 5 °C using two-dimensional ^{1}H−^{15}N HSQC spectra (Figure 3A). At pH 7.4, the HSQC spectrum of F30H-G_{B1} is well dispersed in both the ^{1}H and ^{15}N dimensions, consistent with a folded protein. At pH 3.5, the main chain amide protons are poorly dispersed in the ^{1}H dimension, consistent with an unfolded protein. Between these two extremes of pH, the HSQC spectra show two sets of signals corresponding to the folded and unfolded states in slow exchange. A plot of fraction folded, judged from the peak intensity of the W43 N_ϵH signal, versus pH shows a midpoint near pH 5.5 where the folded and unfolded states are in an approximately 1:1 equilibrium mixture (Figure 3B). Raising the pH back to 7.4 from 3.5 leads to reversible refolding of the protein based on the HSQC spectrum.

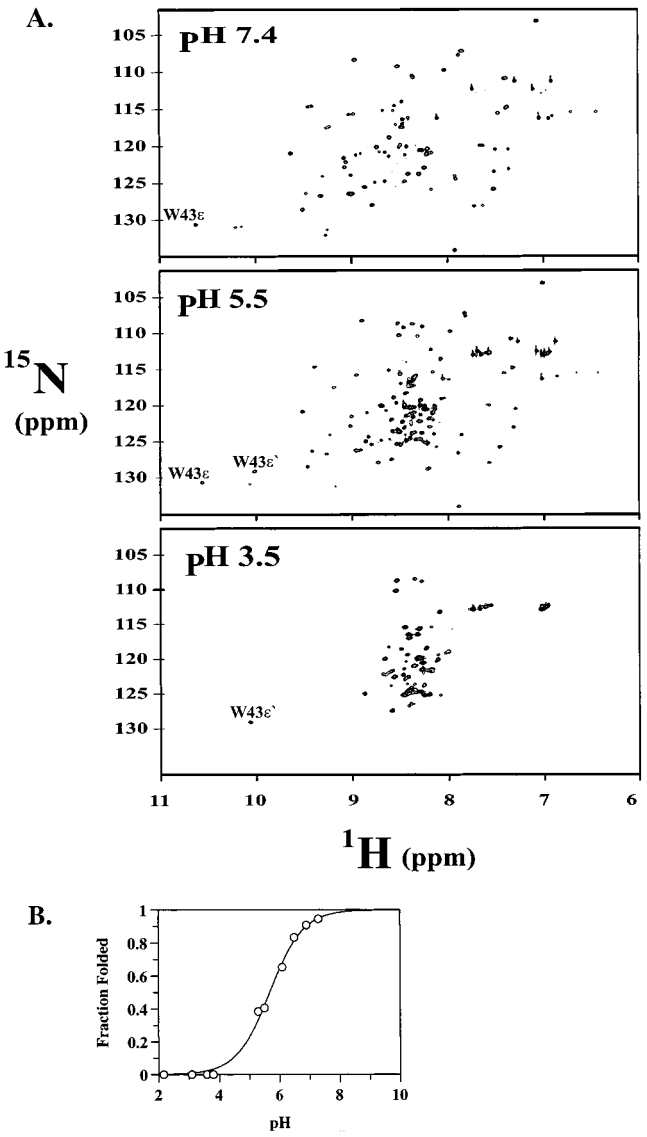

FIGURE 3: (A) $^1H-^{15}N$ HSQC spectra of F30H-G_{B1} as a function of pH at 5 °C. At pH 7.4, the protein is fully folded whereas at pH 3.5 it is denatured. At pH 5.5, a 1:1 mixture of folded and unfolded states exists in slow exchange. The cross-peak due to the W43 indole proton is labeled for both native (W43ϵ) and denatured (W43ϵ') states. (B) Fraction of folded protein versus pH measured at 5 °C from the W43 indole proton peak intensity as a function of pH.

Kinetics of Folding. We have measured the rate of F30H-G_{B1} folding at pH 7.6, 20 °C, as described under Materials and Methods. The protein was denatured at pH 2.3 and then renatured by jumping the pH to 7.6. F30H-G_{B1} contains one tryptophan (W43) which is largely buried in the native state. Thus, the extent of folding can be monitored by an increase in tryptophan fluorescence versus time.

The kinetic curve for refolding of F30H-G_{B1} can be fitted to a first-order equation with a single rate constant of 104 s^{-1} (Figure 4). G_B contains no prolines which could introduce complexity in the refolding rate due to cis−trans isomerization. The residuals of data minus fit are randomly distributed around zero, indicating that no other kinetic phases are observable. By comparison, the folding rate of G_{B1} under these conditions is 180 s^{-1}. Fluorescence increases by a factor of 6.3 during the folding of F30H-G_{B1}. This is the maximum amplitude expected from steady-state fluorescence measurements at pH 2.3 and 7.6. These observations indicate that intermediates which partially bury W43 do not accumulate during the folding reaction of F30H-G_{B1}. Also, while the F30H substitution destabilizes the native state by about 5 kcal mol^{-1}, it has little effect (ca. 0.5 kcal mol^{-1}) on the energy of the transition state for folding.

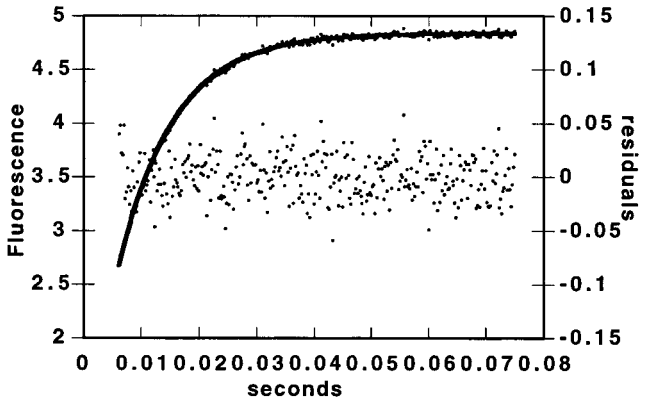

FIGURE 4: Plot of tryptophan fluorescence versus time for F30H-G_{B1} at pH 7.6, 20 °C.

Resonance Assignments in Native and Acid-Denatured F30H-G_{B1}. Backbone and side-chain assignments at pH 7.4, 5 °C, were obtained from 2D homonuclear spectra (TOCSY and NOESY) and 3D heteronuclear spectra (^{15}N NOESY−HSQC and ^{15}N TOCSY−HSQC). Assignments for the acid-denatured state were also made from a combination of experiments. At pH 5.5, exchange cross-peaks were detected between amides in the folded and unfolded states in a 3D ^{15}N NOESY−HSQC spectrum recorded at 5 °C. Using known assignments for folded amides, approximately 40% of the backbone NHs in the unfolded state were assigned from this spectrum. The remaining backbone NH assignments were made using a 3D ^{15}N HMQC−NOESY−HSQC experiment at pH 3.5 (*31*, *57*). This experiment takes advantage of the fact that ^{15}N shifts are well-dispersed even in unfolded proteins (Figure 3A) and uses two ^{15}N dimensions to obtain unambiguous sequential H_N-H_N (i, $i+1$) assignments (Figure 5). In combination with ^{15}N TOCSY−HSQC and NOESY−HSQC spectra, backbone H_α, H_N, and ^{15}N resonance assignments were obtained for 53 out of 56 residues in the acid-denatured state at 5 °C.

Chemical Shifts. The chemical shift index ($\Delta\delta = \delta_{obs} - \delta_{rc}$), a particularly sensitive indicator of secondary structure, was used to compare $^1H_\alpha$ chemical shifts in the native and acid-denatured states with random coil values (*58*−*61*). Corrections were made for nearest-neighbor contributions of aromatic groups using methods described previously (*62*, *63*). Based on the magnitude and direction of the difference $\Delta\delta$, native F30H-G_{B1} has the same secondary structure pattern as wild-type G_{B1} (Figure 6A). For acid-denatured F30H-G_{B1}, the $\Delta\delta$ values are much smaller with maximum values of ±0.2 ppm. This is because residual structures are weakly populated and chemical shifts are a linear average of all conformers present. The results summarized in Figure 6B indicate the presence of some residual nativelike structure in the α-helix. However, the chemical shift data alone do not provide conclusive information about the presence of β-hairpins in the denatured state. ^{15}N and H_N shifts were also compared with their random coil values, but no meaningful conclusions could be made (data not shown). Previous work has sug-

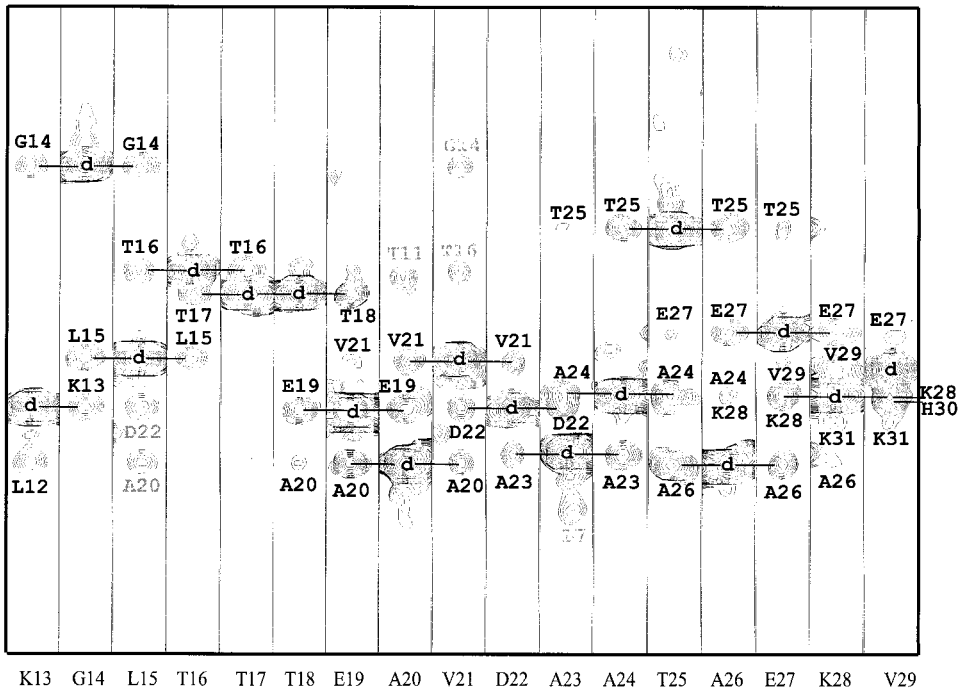

FIGURE 5: Strip plot from a 3D ^{15}N HMQC−NOESY−HSQC spectrum of F30H-G_{B1} at pH 3.5, 5 °C, showing H_N-H_N sequential and nonsequential assignments in a portion of the polypeptide chain. Autopeaks are represented by the letter d. Gray characters indicate spectral overlaps.

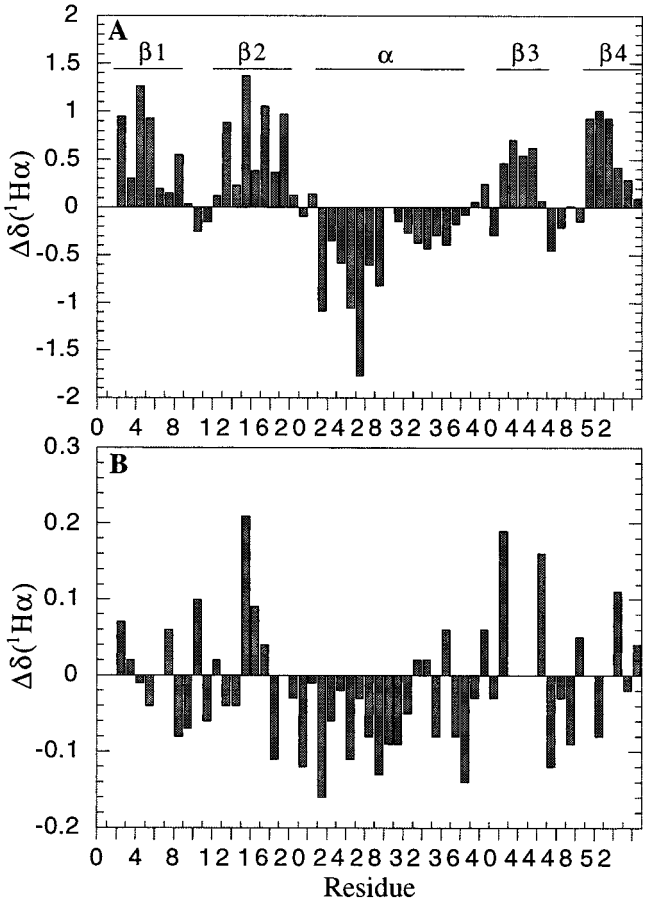

FIGURE 6: Comparison of $\Delta\delta^1H_\alpha$ conformational shifts (observed H_α shift − random coil H_α shift) in F30H-G_{B1} at (A) pH 7.3 (folded) and (B) pH 3.5 (unfolded). Chemical shifts are for data recorded at 5 °C.

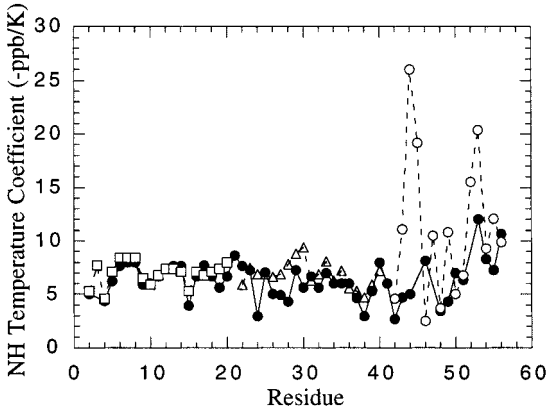

FIGURE 7: Amide proton temperature coefficients (−ppb/K) for F30H-G_{B1} at pH 3.5 (filled circles) and for the peptide fragment from residues 1−20 (open squares), fragment 21−40 (open triangles), and fragment 41−56 (open circles). The peptide fragment data are taken from ref *25*. Both the F30H-G_{B1} and peptide fragment data were measured over a temperature range of 5−35 °C.

gested that these shifts have significant sequence-dependent components that are still not well understood (*62*, *64*).

Amide temperature coefficients were measured for the acid-denatured state at pH 3.5 and were compared with temperature coefficients for peptide fragments corresponding to the $\beta1-\beta2$, α-helix, and $\beta3-\beta4$ regions (*25*). The temperature coefficients in the $\beta1-\beta2$ and α-helical regions of F30H-G_{B1} are similar to those for the corresponding peptide fragments (Figure 7). However, amide temperature coefficients are significantly larger in the $\beta3-\beta4$ peptide fragment than in the corresponding region of F30H-G_{B1}, particularly for T44 and T53. The large values in the peptide fragment are due to a structural transition from folded hairpin to random coil when the temperature is raised from 5 to 35 °C (*25*). Therefore, the smaller temperature coefficients in the $\beta3-\beta4$ region of acid-denatured F30H-G_{B1} suggest that the nascent $\beta3-\beta4$ hairpin conformation is more stable in the full-length polypeptide chain than in the isolated peptide

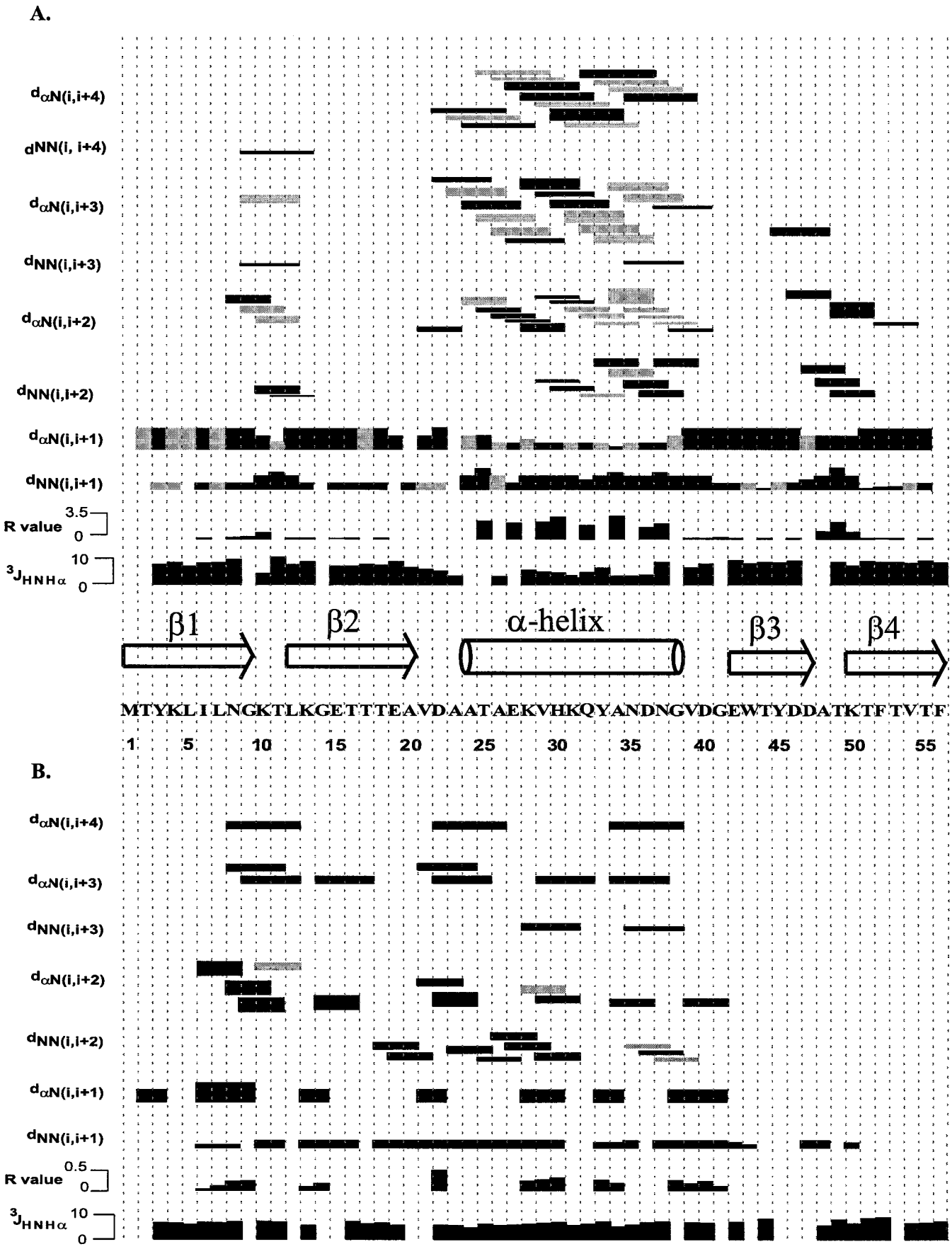

FIGURE 8: Summary of backbone NOE connectivities and $^3J_{HNH\alpha}$ values for F30H-G_{B1} at (A) pH 7.5 and (B) pH 3.5, at 5 °C. The *R*-value is defined as the ratio of the intensity of $d_{NN}(i, i+1)$ to the intensity of $d_{\alpha N}(i, i+1)$. Elements of secondary structure are shown above the protein sequence. The thickness of the NOE connectivities reflects the relative NOE intensities observed in 250 ms mixing time 3D ^{15}N NOESY−HSQC and ^{15}N HMQC−NOESY−HSQC spectra. Gray lines refer to ambiguities in the measurements due to resonance overlap.

fragment. Further data, described under Discussion, also support this idea.

NOEs. For native F30H-G_{B1}, the sequential $d_{\alpha N}(i, i+1)$ and $d_{NN}(i, i+1)$ connectivities are consistent with a wild-type G_{B1} fold (Figure 8A). Strong $d_{\alpha N}(i, i+1)$ and weak $d_{NN}(i, i+1)$ NOEs are observed for residues 3−9, 12−20, 42−46, and 51−55, corresponding to β-strand regions (*65*). Strong $d_{NN}(i, i+1)$ and weak-to-medium $d_{\alpha N}(i, i+1)$ NOEs are detected for residues 10−11, 24−38, and 47−50, corresponding to turn/helix regions. Further support for a wild-type global fold is evident from NOEs involving side chains (not shown).

In acid-denatured F30H-G_{B1}, sequential $d_{\alpha N}$ and d_{NN} NOEs are observed throughout the polypeptide chain as in other unfolded proteins (e.g., see refs *36*, *38*). However, these sequential NOEs have limited meaning in both short peptides and unfolded proteins as they can be satisfied by multiple conformational states. A more useful parameter is the *R*-value, where *R* is the intensity of $d_{NN}(i, i+1)$/intensity of $d_{\alpha N}(i, i+1)$. This provides a measure of the residues populating the α-region of (ϕ,ψ)-space (*36*, *66*). The *R*-values show that the acid-denatured state contains some residual turn/helix structure for residues 8, 9, 14, 22, 28−30, 33, 34, and 38−40 (Figure 8B). Additional *R*-values could not be obtained due to peak overlap or line broadening. Residual turn/helix structure is further supported by a series of nonsequential (i, $i+2$), (i, $i+3$), and (i, $i+4$) $d_{\alpha N}$ and d_{NN} NOEs for residues 8, 9, 14, 18, 19, 21−23, 25−29, 34−36, and 39 (Figure 8B and Figure 9). Further unambiguous NOEs in the helical region could not be obtained due to peak overlap. It is interesting to note that a number of d_{NN} and $d_{\alpha N}(i, i+2)$ and (i, $i+3$) connectivities detected in the acid-denatured state are not observed in the folded state. Specifically, the NOEs $I6H_\alpha-N8H_N$, $N8H_\alpha-T11H_N$, $N8H_\alpha-L12H_N$, $G14H_\alpha-T16/T17H_N$, $T18H_N-A20H_N$, $E19H_N-V21H_N$, and $V39H_\alpha-G41H_N$ are non-native (Figure 9).

Short-range NOEs cannot be used to distinguish between β-sheet and random coil structure since both populate the same region of (ϕ,ψ)-space (*67*, *68*). The only unambiguous way to define β-sheet regions is through the use of long-range interstrand NOEs. In this study, only one clear-cut long-range NOE, from $G41H_\alpha$ to $T55H_N$, was detected (Figure 9), and this NOE also occurs in the native state. This part of the polypeptide chain is therefore loosely constrained to β-hairpin type conformations. No additional interstrand NOEs are observed in this region, and amide proton signals for residues 42−55 are significantly line broadened at 5 °C where these NOE experiments were carried out (see below). The amide signals for these residues are slightly more intense at 20 °C, but still no other interstrand NOEs could be detected in this part of the polypeptide chain.

Coupling Constants. Coupling constants were obtained from a 3D HNHA experiment using the method of Vuister and Bax (*53*). For the folded state at pH 7.5 and 5 °C, the coupling constants are consistent with the secondary and tertiary structure determined from chemical shifts and NOEs (see above). Typical $^3J_{HNH\alpha}$ values are in the 8−11 Hz range for residues in β-strands and 4−7 Hz for residues in the α-helix (Figure 8A). An exception is N37 in the C-terminus of the helix which has a $^3J_{HNH\alpha}$ coupling constant of 10 Hz. This is similar to the $^3J_{HNH\alpha}$ value obtained for this residue in a G_{B2} domain using 2D DQF−COSY and HMQC-J spectra (*8*).

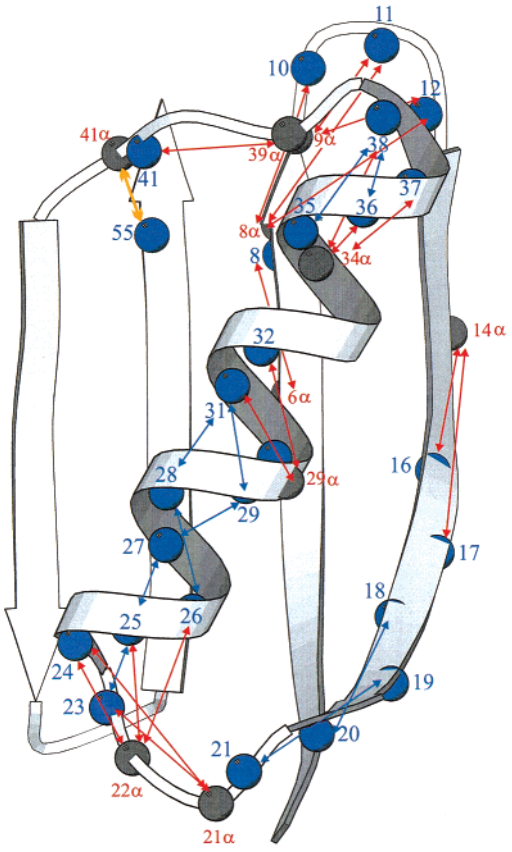

FIGURE 9: Summary of the nonsequential backbone NOEs in acid-denatured F30H-G_{B1} at pH 3.5, 5 °C, superimposed on the native structure of G_{B1}. Blue spheres indicate main chain amide nitrogens. Gray spheres indicate main chain C_α atoms. Nonsequential $d_{\alpha N}$ NOE connectivities are represented with red lines while d_{NN} contacts are shown in blue. The long-range NOE from G41 H_α to T55 H_N is shown in yellow. Only unambiguous NOEs are displayed.

For the acid-denatured state at pH 3.5 and 5 °C, $^3J_{HNH\alpha}$ values range from 5.2 to 9.7 Hz (Figure 8B). Residues corresponding to the α-helix region in the folded state also have relatively low $^3J_{HNH\alpha}$ values in the acid-denatured state ranging from 5.2 to 7.9 Hz. However, these coupling constants are not as low as in the folded state due to rapid exchange with random coil conformations. The highest coupling constants in this region are for Y33 (7.9 Hz) and N37 (7.9 Hz). Four residues have $^3J_{HNH\alpha}$ values greater than 8 Hz: T44 (9.2 Hz), T49 (8.8 Hz), T51 (9.5 Hz), and F52 (9.7 Hz), consistent with population of extended β-strand type conformations. These all occur in the region corresponding to the $\beta3-\beta4$ hairpin in the folded state. The $^3J_{HNH\alpha}$ coupling constants also appear to depend on residue type to some extent (Figure 10), with alanine residues giving consistently lower ^3J values as observed previously (*36*, *38*, *65*, *69*).

Line Broadening. Peak intensities were used as indicators of line broadening effects in analogy with the work of Wong et al. (*38*). The intensities of all HSQC peaks increase as the temperature is raised to 20 °C (Figures 11 and 12). However, the profile for the intensity versus residue number curve is similar at both 0 °C and 20 °C. The most intense peaks are in a region corresponding to the β2-strand in the folded protein and containing non-native turn-like interactions in the unfolded state. A decrease in peak intensity is observed toward the C-terminus, with residues 42−55 having the most

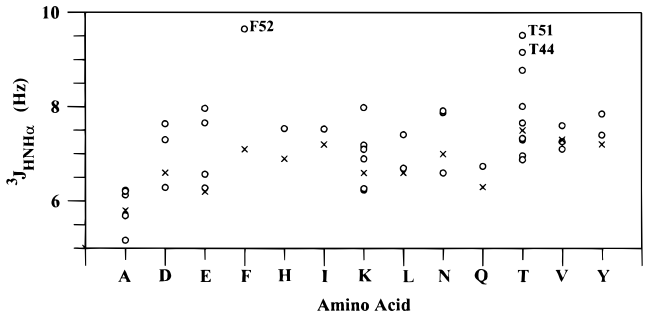

FIGURE 10: Plot of $^3J_{HNH\alpha}$ coupling constants versus amino acid residue type. Open circles denote the experimental data obtained for F30H-G_{B1} in its acid-denatured state (pH 3.5) at 5 °C, and crosses correspond to the predicted $^3J_{HNH\alpha}$ values for each residue type in the random coil state (*69*). The most notable differences from random coil values are observed for residues T44, T51, and F52.

significant line broadening. Our results are different from those for the cold-denatured state of barstar where peak intensities are higher at the N- and C-termini of the polypeptide chain, and the highest intensities are observed at the C-terminal region (*38*).

Steady-State {$^1H-^{15}N$} NOEs. Backbone flexibility was probed for individual residues in the acid-denatured state on the picosecond to nanosecond time scale using {$^1H-^{15}N$} steady-state NOE measurements as a function of temperature from 5 to 40 °C (Figure 13). Positive {$^1H-^{15}N$} steady-state NOEs indicate regions of restricted backbone motions proportional to the size of the NOE, while negative values indicate regions with rapid (<1 ns) large-amplitude backbone motions. At 5 °C, positive NOEs (0.1−0.4) are observed for residues 10, 22−48, and 54−55, indicating that these are the most conformationally restricted parts of the polypeptide chain. These residues are located in the $\beta1-\beta2$ turn, the helix−loop−$\beta3$ region, and the C-terminus of the $\beta4$-strand, respectively, in the folded state (Figure 14). Negative NOEs (−0.1 to −0.8) are detected for residues 2−6, 50−52, and 56. These residues are in regions corresponding to the $\beta1$-strand and $\beta4$-strand of the folded state, respectively.

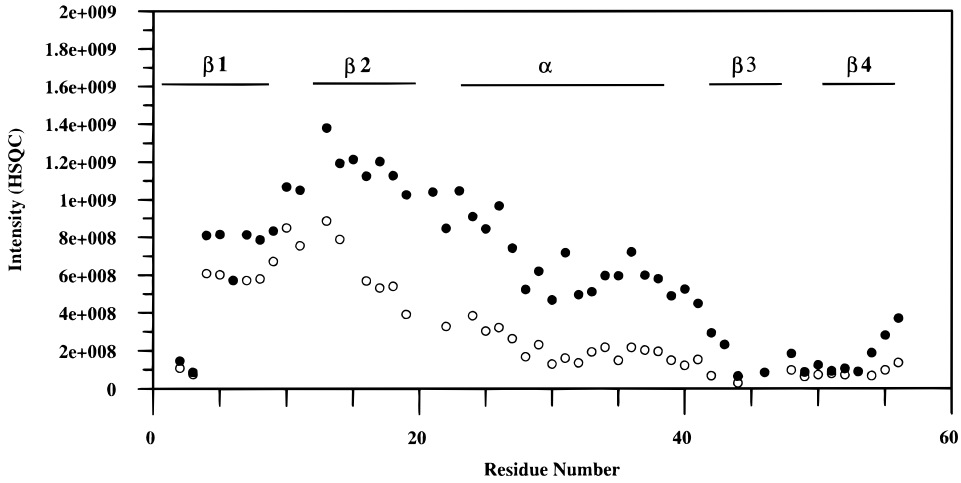

FIGURE 11: Plot of amide peak intensities from HSQC spectra in arbitrary units versus residue number for acid-denatured F30H-G_{B1} at pH 3.5. Peak intensities were measured at 0 °C (open circles) and 20 °C (filled circles).

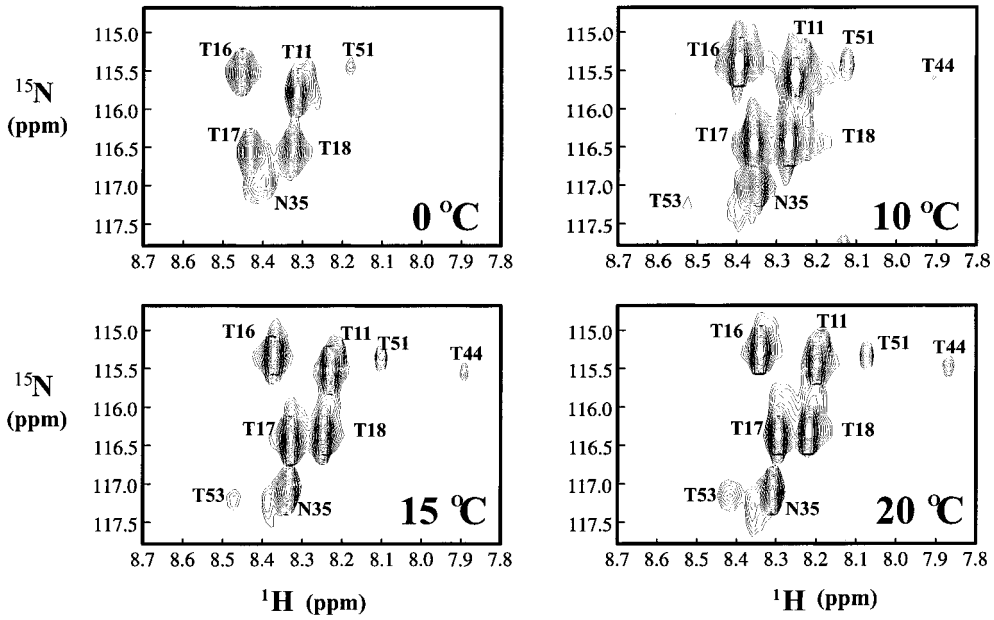

FIGURE 12: Section of the $^1H-^{15}N$ HSQC spectrum of acid-denatured F30H-G_{B1} (pH 3.5) as a function of temperature, demonstrating the wide variation in peak intensities. The amide signals of T44, T51, and T53 are significantly line broadened and have low intensity, even at 20 °C, while the other resonances in this section maintain relatively narrow line widths.

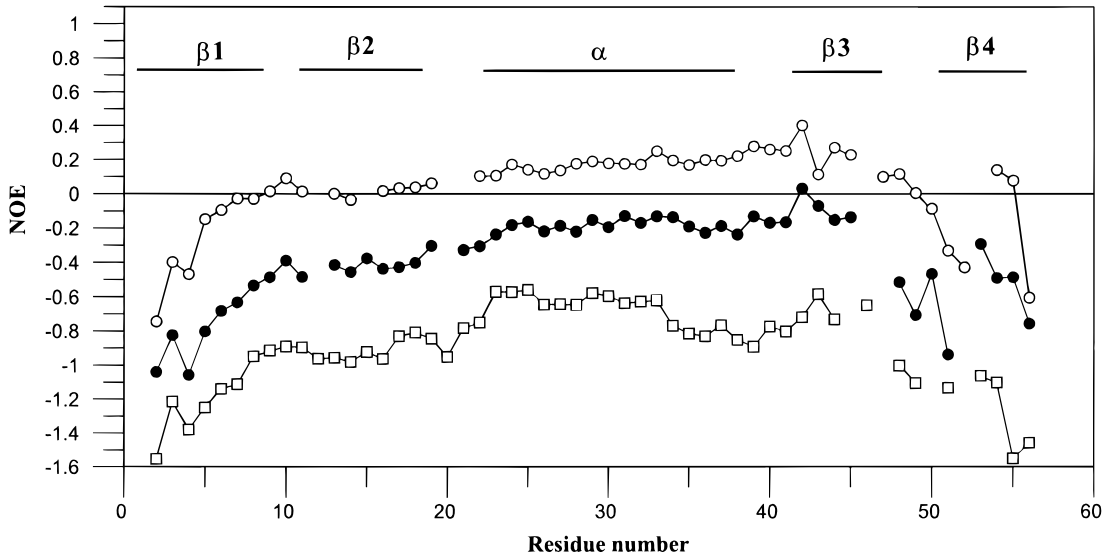

FIGURE 13: Plot of backbone steady-state {^{1}H−^{15}N} NOEs versus residue number for acid-denatured F30H-G_{B1} at pH 3.5. The heteronuclear NOEs were measured at 5 °C (open circles), 25 °C (filled circles), and 40 °C (open squares).

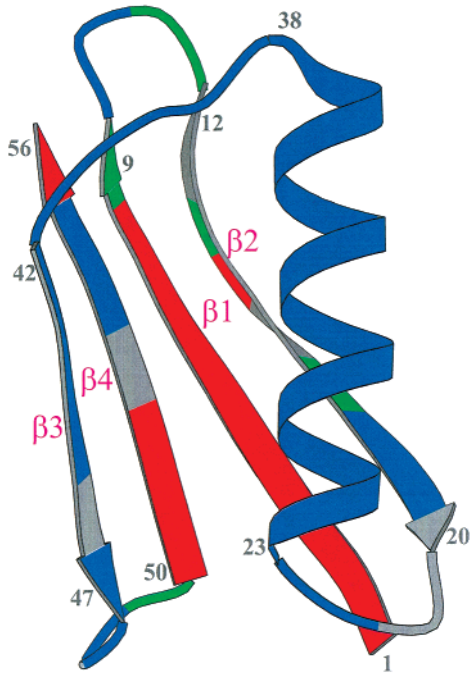

FIGURE 14: Summary of backbone steady-state {^{1}H−^{15}N} NOEs for acid-denatured F30H-G_{B1} at pH 3.5, 5 °C, superimposed on the native structure of G_{B1}. Heteronuclear NOEs are color-coded as follows: residues with negative NOEs are in red, residues with zero NOEs (−0.02 to +0.02) are in green, and residues with positive NOEs are in blue. Regions for which no NOE data could be obtained are in gray.

At 25 °C, nearly all {^{1}H−^{15}N} NOEs are negative with a pattern similar to the 5 °C data, indicating that the backbone dynamics profile is preserved despite the increased mobility (Figure 13). At 40 °C, NOEs are more negative (∼−1.0) than they are at 25 °C (∼−0.4), and the pattern changes, particularly at the C-terminus where residues 48 and 51 now have similar NOEs and residue 55 has a strong negative NOE. The results at 40 °C show that there are increased large-amplitude motions (∼1 ns) everywhere in the protein relative to the 5 °C and 25 °C data, with more mobility at the C- and N-termini, a common feature for unfolded proteins (*41*, *70*−*74*).

DISCUSSION

Residual Structure in the Acid-Denatured State. The F30H mutation in G_{B1} provides a convenient switch for reversibly unfolding protein G under relatively mild, weakly folding conditions. This mutant unfolds as the pH is lowered below 7, presumably due to protonation of the H30 residue, with a pH midpoint around 5.5 at 5 °C. This midpoint is close to the pK_a for a solvent-exposed histidine. Since the F30H mutant is thermally destabilized relative to wild-type, it is likely that the H30 group is transiently solvent-exposed. Protonation of this transient species would then shift the equilibrium toward the unfolded state. Denatured states studied under such weakly folding conditions have been shown to be more structured than in the presence of chaotropic reagents (*30*, *35*, *36*). Moreover, these weakly folding conditions may be more relevant to protein folding in vivo.

In such denatured states, polypeptide chain conformations are an ensemble average, but one can obtain conformational preferences for this ensemble utilizing information from chemical shifts, coupling constants, and NOEs. Residual structure, defined here as any deviation from random coil (ϕ,ψ)-space, is likely to be weakly populated, and parameters obtained are a weighted average which is dominated by the random coil contribution to the ensemble. In the case of chemical shifts, this weighting is a linear average, and therefore deviations from random coil values are typically quite small. Similarly, $^3J_{HNH\alpha}$ values are not usually a sensitive indicator of residual structure in unfolded proteins (e.g., see ref *38*). However, the NOE has a $1/r^6$ bias toward the observation of short distances (<5 Å) and represents the best chance of detecting residual structure in unfolded states of proteins. Therefore, there may be cases where the chemical shift and coupling constant effects are small but NOE evidence exists for residual structure. In combination, the chemical shift, coupling constant, and NOE provide a useful way of defining the structural characteristics of a denatured state.

Previous studies demonstrated that the urea-denatured state of G_{B1} is a random coil with no detectable residual structure (*41*). In contrast, our results indicate that the acid-denatured state of F30H-G_{B1} has conformations that deviate measurably

from random coil (ϕ,ψ)-space. Nativelike residual structure is present in regions corresponding to the $\beta1-\beta2$ turn (residues 9−12), the α-helix (residues 22−38), and the $\beta3-\beta4$ hairpin (residues 42−56) in folded protein G. A number of non-native turn-like interactions are also present in regions corresponding to the $\beta1$-strand (residues 6−9), the $\beta2$-strand (residues 14−17 and 18−21), and the $\alpha-\beta3$ loop (residues 39−41) in the folded state. Therefore, considerable residual structure exists in the acid-denatured state with only residues 1−5 in the $\beta1$ region being characterized as essentially random coil.

Line Broadening. A variable-temperature study on the unfolded F30H-G_{B1} mutant at pH 3.5 reveals line broadening of some amide signals in HSQC spectra recorded at low temperatures. At 0 °C, a number of HSQC peaks are severely line broadened due to intermediate exchange between conformers with respect to the microsecond−millisecond time scale of the NMR experiment. As the temperature is raised, this conformational exchange is more rapid, and the corresponding line widths become narrower (Figure 12). The unfolded state is an ensemble of multiple conformations that are in equilibrium with each other. The slower exchange between some conformational substates at low temperatures is due to their relative stabilization in the unfolded protein (cf. ref *36*).

The most significant line broadening is seen for C-terminal residues 42−55 in F30H-G_{B1}. This region of the polypeptide chain corresponds to the $\beta3-\beta4$ hairpin in the folded state. The observation of line broadening suggests that this region is conformationally restricted in the acid-denatured state. Further, coupling constants and NOEs suggest that this region preferentially populates nativelike conformations. Therefore, the $\beta3-\beta4$ hairpin region has a slowed rate of exchange with other conformers in the ensemble representing the acid-denatured state. In contrast, other structured regions such as the $\beta1-\beta2$ turn and the non-native turn-like structures in the $\beta2$ region are in relatively fast exchange with extended (unstructured) conformers and do not have broadened lines. Helical residues have somewhat broadened lines but not to the extent of the $\beta3-\beta4$ hairpin region, and therefore their exchange rates with extended conformations are between those for the $\beta3-\beta4$ and $\beta1-\beta2$ regions.

This type of line broadening has been observed in a number of other NMR studies of denatured proteins and corresponds with more structured regions that are in intermediate exchange with extended conformations (*32*, *35*, *36*, *38*). For example, line broadening is seen in cold-denatured barstar for residues in regions associated with residual structure (*38*). Line broadening is also observed at low temperatures for residues 23−28 of the U_{exch} state of drkN SH3 domain (*36*). These residues are in a non-native turn-like structure. Mok et al. (*37*) argue that the presence of this stable non-native structure reduces the stability of the folded state and this is the reason the domain has low stability compared to other SH3 domains. In acid-denatured F30H-G_{B1}, the most stable residual structure is the nativelike $\beta3-\beta4$ hairpin. Wrabl and Shortle (*75*) showed that a perturbation that enhances a native interaction in denatured states always increases the stability of the native state. The presence of such stabilized nativelike interactions in the acid-denatured state of F30H-G_{B1} is therefore consistent with the high stability of the native state for wild-type G_{B1} (*13*).

It should also be noted that these line broadening effects are not present when chemical denaturants are used for protein G (*41*) and the drkN SH3 domain (*35*, *36*). In these cases, chaotropic agents such as urea and guanidine hydrochloride disrupt residual structure, and the unfolded states more closely resemble a random coil.

Backbone Dynamics. To study the backbone dynamics of the F30H-G_{B1} mutant, a set of variable-temperature $\{^1H-^{15}N\}$ steady-state NOE experiments was recorded. The model-free approach (*76*−*78*), in which the protein is assumed to be diffusing isotropically in solution with a single correlation time, was not used in this analysis. This is because unfolded proteins do not fit into this description very well due to additional anisotropy and flexibility introduced when the protein unfolds. $\{^1H-^{15}N\}$ steady-state NOE experiments provide qualitative information about protein backbone dynamics, and this information proved to be useful in our efforts to understand the folding of protein G.

Since our structural analysis was carried out at 5 °C, we review here the 5 °C steady-state $\{^1H-^{15}N\}$ NOE data in detail. For the most part, the regions of the denatured protein with residual structure at 5 °C also show restricted backbone flexibility on the nanosecond to picosecond time scale as evidenced by positive heteronuclear NOEs. The most restricted backbone motions occur in residues corresponding to the $\beta1-\beta2$ turn, the α-helix, the $\alpha-\beta3$ loop, the $\beta3$-strand, and parts of the $\beta4$-strand in the folded state (Figure 14). More backbone flexibility occurs in the $\beta2$ region where nonnative structure is detected in the denatured state, and the most flexible regions are the N-terminal residues 1−6, the C-terminal residue 56, and residues 51 and 52. The N- and C-terminal residues are typically more flexible in unfolded proteins, so the negative heteronuclear NOEs for residues 1−6 and 56 are not surprising (*41*, *70*−*74*). On the other hand, residues 51 and 52 are in the $\beta4$ region, which is believed to have restricted conformational sampling based on line broadening data. In addition, the $^3J_{HNH\alpha}$ coupling constants for T51 and F52 are both greater than 9 Hz, indicating that these residues prefer conformations in the β-region of (ϕ,ψ)-space despite their greater flexibility than other residues in the nascent $\beta3-\beta4$ hairpin of the acid-denatured state. This flexibility may be due to concerted motion of residues 51 and 52 on the picosecond to nanosecond time scale in such a way that β-conformers are still preferred.

It is interesting to note that while residues 51 and 52 have negative NOEs (−0.4 to −0.5), residues V54 and T55 have positive NOEs (ca. 0.2), indicating significant differences in backbone dynamics along this section of the polypeptide chain. No data could be obtained for T53 at 5 °C. The structural data show that residues 41−55 are loosely constrained in a β-hairpin-like conformation, and the heteronuclear NOE results indicate that the ends of this incipient hairpin are more ordered than residues 51 and 52 of the interior (Figure 14). To form a stable hairpin, residues W43, Y45, F52, and V54 need to form a series of favorable hydrophobic interactions with each other. In the acid-denatured state, these interactions are not likely to be fully developed, and the hydrophobic contacts between W43 and V54 may be more stabilizing than those between Y45 and F52. While hairpin formation is most likely initiated from the β-turn, recent work has suggested that it may also

start by clustering of hydrophobic residues to form a loop (*79*). Our results say nothing about folding kinetics, but they are at least consistent with a picture of the nascent β-hairpin having more ordered interactions at its ends than the interior.

Comparison with Peptide Fragment Studies. A number of CD and NMR studies have been carried out in water and water/trifluoroethanol (TFE) on peptide fragments corresponding to the $\beta1-\beta2$ hairpin (residues 1−20), the α-helix (residues 22−38), and the $\beta3-\beta4$ hairpin (residues 41−56) (*23*−*26*). Fragments corresponding to residues 2−19 (*24*) and 1−20 (*25*) of the $\beta1-\beta2$ hairpin have been shown to be mostly random coil in water with some turn conformations from residues 6−10 and residues 14−15. In contrast, our data show more extensive turn structures from residues 6−12, residues 14−17, and residues 18−21 in fast exchange with random coil conformations. Nativelike NOEs corresponding to the $\beta1-\beta2$ turn (residues 9−12) are detected in the acid-denatured state of F30H-G_{B1} which do not appear in the peptide fragments in water.

Fragments corresponding to residues 21−40 (*25*) and 19−41 (*26*) give differing results. Fragment 21−40 is essentially random coil in aqueous solution with very little helical content (∼5%). Fragment 19−41, on the other hand, has helical structure from residues 22−32, and V21 forms a non-native hydrophobic staple with A26 which stabilizes the N-terminal half of the helix. These structures are in rapid exchange with random coil conformations. In the acid-denatured state of F30H-G_{B1}, our results indicate that helix/turn conformations persist from residues 22−32 and residues 34−38 with a number of (i, i+2), (i, i+3), and (i, i+4) NOEs being detected (Figures 8 and 9). Although the V21−A26 interaction is not observed, an (i, i+4) NOE contact from D22 to A26 is detected and non-native turn structures are found for residues 18−21 leading into this region, as described above. The C-terminal half of the helix is therefore considerably more structured in the acid-denatured polypeptide, and residues 34−39 correspond to a stabilizing Schellman motif in the native state. Further, a non-native turn structure is detected at the C-terminal end of the helix for residues 39−41 in acid-denatured F30H-G_{B1}.

Fragment 41−56 (*23*, *25*) corresponds to the $\beta3-\beta4$ hairpin and has nativeike structure in water (∼40% β-hairpin from CD). The resonances are quite narrow, indicating rapid exchange with random coil conformations. In contrast, amide resonances in the $\beta3-\beta4$ region of acid-denatured F30H-G_{B1} are significantly line broadened and are in intermediate exchange with extended structures. The slowed conformational exchange in F30H-G_{B1} indicates that the $\beta3-\beta4$ hairpin structure is more stabilized in the full-length polypeptide chain than in the peptide fragment. These results, along with earlier amide temperature coefficient data, suggest additional medium-to-long-range interactions in the longer polypeptide chain that are not present in the peptide fragments in water. The comparisons underscore the difficulty of using peptide fragments where truncation of the chain by only one or two residues can have large effects on structure. It is also interesting to note that the use of water/TFE in the peptide fragment studies leads to increased structure in the α-helix and β-hairpins and it is thought that the presence of TFE may strengthen intramolecular hydrogen bonds (*80*) and mimic the interior of a protein (*81*).

There is no direct NOE evidence for longer range interactions between secondary structure motifs in the acid-denatured state, but such contacts, even if transient, would lead to mutual stabilization of the interacting regions. Nativelike interactions between (1) the hydrophobic faces of the nascent $\beta3-\beta4$ hairpin and the N-terminal half of the α-helix and (2) the C-terminus of the helix and the $\beta1-\beta2$ turn would help to explain the enhanced stability and structure of these regions in the acid-denatured state relative to the peptide fragments. Further non-native contacts may also be possible. However, these interactions are limited to intramolecular events since more dilute samples of F30H-G_{B1} exhibit identical NMR characteristics.

Implications for Folding. The mechanism for how protein folding gets started is still not well understood. Characterization of initiation sites on the polypeptide chain in real time has proved to be difficult due to their transient nature. Pulse-labeling experiments, for example, cannot probe folding events that occur faster than the dead time of the quench flow mixing device, typically 1−5 ms. In the case of G_B, as well as other small proteins exhibiting two-state kinetics (*14*), much of the folding reaction occurs within the dead time, and little is known about the very early events occurring in this burst phase (*16*). Recent elegant studies of peptide fragments using laser temperature-jump experiments indicate that helices can form on the order of nanoseconds to microseconds and that β-hairpins form about 30 times more slowly (*79*, *82*, *83*). This optical method provides important information about macroscopic folding events, but details about the folding kinetics of specific residues are more difficult to obtain. In this regard, NMR studies of denatured states under equilibrium conditions can provide significant insights into protein folding and stability. While they do not give kinetic information, any residual structures that are detected in the denatured state are potential initiation sites for protein folding.

Based on our NMR results, we can develop a model for the acid-denatured state and provide plausible scenarios in the early folding of protein G which can subsequently be tested using a combination of mutagenesis and kinetic studies. Although the acid-denatured state consists of multiple conformers in rapid exchange with each other, localized parts of the polypeptide chain clearly prefer certain regions in (ϕ,ψ)-space over others. Nativelike conformational preferences in the $\beta3-\beta4$ hairpin, the α-helix, and the $\beta1-\beta2$ turn suggest that there may be multiple sites for the initiation of folding. This high degree of preference for nativelike conformers in the denatured state may help to explain the rapid kinetics of folding protein G (*14*).

A number of turn-like conformations are also detected in the denatured state which do not appear in the corresponding regions of the folded state. Similar observations have been made in studies on barstar (*38*) and the drkN SH3 domain (*35*−*37*). Turns have been shown to provide nucleation sites for protein folding (*84*). Dyson et al. (*85*) showed that some turn structures could be partially maintained in small peptide fragments in the absence of the complete polypeptide sequence. These sites are presumably important in restricting conformational space at an early stage in folding, thereby allowing the polypeptide chain to explore productive conformations leading to a stably folded protein more efficiently. Even non-native turn structures may therefore be useful in

that they restrict further extension of the polypeptide chain. Two of the four non-native turn conformations in acid-denatured F30H-G_{B1} are in the region corresponding to the β2-strand of the native state. Thus, the intrinsic propensity of this region of the polypeptide chain is to form off-pathway helix/turn structures rather than β-conformations. In light of this result, it is interesting to note that the β2-strand is the least stable in the β-sheet as measured from hydrogen exchange rates of backbone amide protons (*17*). The hydrogen exchange data suggest that the β2-strand unfolds more readily than the rest of the β-sheet while the present study suggests slower folding of the β2-strand since competing non-native structures would need to unfold before refolding to the native state could be achieved. Thus, structural studies of denatured states also appear to provide clues as to which regions may fold more slowly. These ideas could be further tested with mutagenesis and kinetic studies.

Comparison with Theoretical Calculations. Finally, it is worth comparing our experimental results with a recent molecular dynamics study on the full-length polypeptide chain of G_{B1} (*86*). In this theoretical model, high-probability native contacts are detected for the following regions in the early stages of folding: (1) residues 22−33 of the α-helix; (2) the β3−β4 turn; and (3) N37−L7, i.e., between the C-terminus of the helix and the β1-strand. The observation of early α-helix and β3−β4 turn formation is consistent with our experimental observations on the acid-denatured state of F30H-G_{B1}, but we cannot detect an interaction between the N37 and L7 side chains. However, we do observe some structure in the regions of N37 and L7 which is not present in the corresponding peptide fragments, suggesting the possibility of similar long-range stabilizing interactions in the full-length polypeptide chain. Perhaps the most notable difference from our NMR work is the absence of non-native conformations during the course of folding in the molecular dynamics study. These interactions may well play a significant role in folding by further restricting the conformational search problem. Equilibrium NMR studies of denatured states therefore provide important experimental results which should be useful in further refinement of computer simulations of protein folding processes.

ACKNOWLEDGMENT

We thank Drs. Alex Drohat, Diane Hancock, and John Marino for help in implementing a number of the pulse programs described here.

REFERENCES

1. Myhre, E. B., and Kronvall, G. (1977) *Infect. Immun. 17*, 475−482.
2. Myhre, E. B., and Kronvall, G. (1981) in *Basic Concepts of Streptococci and Streptococcal Diseases* (Holm, S. E., and Christensen, P., Eds.) pp 209−210, Redbook Ltd., Chertsey Surrey, U.K.
3. Reis, K. J., Ayoub, E. M., and Boyle, M. D. P. (1984) *J. Immunol. 132*, 3098−3102.
4. Fahnestock, S. R., Alexander, P., Nagle, J., and Filpula, D. (1986) *J. Bacteriol. 167*, 870−880.
5. Filpula, D., Alexander, P., and Fahnestock, S. R. (1987) *Nucleic Acids Res. 15*, 7210.
6. Åkerstrom, B., and Bjorck, L. (1986) *J. Biol. Chem. 261*, 10240−10247.
7. Gronenborn, A. M., Filpula, D. R., Essig, N. Z., Achari, A., Whitlow, M., Wingfield, P. T., and Clore, M. G. (1991) *Science 253*, 657−661.
8. Lian, L.-Y., Derrick, J. P., Sutcliffe, M. J., Yang, J. C., and Roberts, G. C. K. (1992) *J. Mol. Biol. 228*, 1219−1234.
9. Orban, J., Alexander, P., and Bryan, P. (1992) *Biochemistry 31*, 3604−3611.
10. Achari, A., Hale, S. P., Howard, A. J., Clore, G. M., Gronenborn, A. M., Hardman, K. D., and Whitlow, M. (1992) *Biochemistry 31*, 10449−10457.
11. Gallagher, T. D., Alexander, P., Bryan, P., and Gilliland, G. (1994) *Biochemistry 33*, 4721−4729.
12. Derrick, J. P., and Wigley, D. B. (1994) *J. Mol. Biol. 243*, 906−918.
13. Alexander, P., Fahnestock, S., Lee, T., Orban, J., and Bryan, P. (1992) *Biochemistry 31*, 3597−3603.
14. Alexander, P., Orban, J., and Bryan, P. (1992) *Biochemistry 31*, 7243−7248.
15. Orban, J., Alexander, P., and Bryan, P. (1994) *Biochemistry 33*, 5702−5710.
16. Kuszewski, J., Clore, G. M., and Gronenborn, A. M. (1994) *Protein Sci. 3*, 1945−1952.
17. Orban, J., Alexander, P., Bryan, P., and Khare, D. (1995) *Biochemistry 34*, 15291−15300.
18. O'Neil, K. T., Hoess, R. H., Raleigh, D. P., and DeGrado, W. F. (1995) *Proteins: Struct., Funct., Genet. 21*, 11−21.
19. Khare, D., Alexander, P., Antosiewicz, J., Bryan, P., Gilson, M., and Orban, J. (1997) *Biochemistry 36*, 3580−3589.
20. Park, S. H., O'Neil, K. T., and Roder, H. (1997) *Biochemistry 36*, 14277−14283.
21. Malakauskas, S. M., and Mayo, S. L. (1998) *Nat. Struct. Biol. 5*, 470−475.
22. Khare, D., Alexander, P., and Orban, J. (1999) *Biochemistry 38*, 3918−3925.
23. Blanco, F. J., Rivas, G., and Serrano, L. (1994) *Nat. Struct. Biol. 1*, 584−590.
24. Blanco, F. J., Jimenez, M. A., Pineda, A., Rico, M., Santoro, J., and Nieto, J. L. (1994) *Biochemistry 33*, 6004−6014.
25. Blanco, F. J., and Serrano, L. (1995) *Eur. J. Biochem. 230*, 634−649.
26. Blanco, F. J., Ortiz, A. R., and Serrano, L. (1997) *Folding Des. 2*, 123−133.
27. Dyson, H. J., and Wright, P. E. (1993) *Curr. Opin. Struct. Biol. 3*, 60−65.
28. Neri, D., Billeter, M., Wider, G., and Wuthrich, K. (1992) *Science 257*, 1559−1563.
29. Arcus, V. L., Vuilleumier, S., Freund, S. M., Bycroft, M., and Fersht, A. R. (1994) *Proc. Natl. Acad. Sci. U.S.A. 91*, 9412−9416.
30. Arcus, V. L., Vuilleumier, S., Freund, S. M., Bycroft, M., and Fersht, A. R. (1995) *J. Mol. Biol. 254*, 305−321.
31. Freund, S. M. V., Wong, K.-B., and Fersht, A. R. (1996) *Proc. Natl. Acad. Sci. U.S.A. 93*, 10600−10603.
32. Alexandrescu, A. T., Abeygunawardana, C., and Shortle, D. (1994) *Biochemistry 33*, 1063−1072.
33. Shortle, D., Wang, Y., Gillespie, J. R., and Wrabl, J. O. (1996) *Protein Sci. 5*, 991−1000.
34. Logan, T. M., Theriault, Y., and Fesik, S. W. (1994) *J. Mol. Biol. 236*, 637−648.
35. Zhang, O., and Forman-Kay, J. D. (1995) *Biochemistry 34*, 6784−6794.
36. Zhang, O., and Forman-Kay, J. D. (1997) *Biochemistry 36*, 3959−3970.
37. Mok, Y. K., Kay, C. M., Kay, L. E., and Forman-Kay, J. (1999) *J. Mol. Biol. 289*, 619−638.
38. Wong, K.-B., Freund, S. M. V., and Fersht, A. R. (1996) *J. Mol. Biol. 259*, 805−818.
39. Fong, S., Bycroft, M., Clarke, J., and Freund, S. M. (1998) *J. Mol. Biol. 278*, 417−429.
40. Eliezer, D., Yao, J., Dyson, H. J., and Wright, P. E. (1998) *Nat. Struct. Biol. 5*, 148−155.
41. Frank, M. K., Clore, G. M., and Gronenborn, A. M. (1995) *Protein Sci. 4*, 2605−2615.

42. Kunkel, T. A., Roberts, J. D., and Zakour, R. A. (1987) *Methods Enzymol. 154*, 367−382.
43. Delaglio, F., Grzesiek, S., Vuister, G. W., Zhu, G., Pfeifer, J., and Bax, A. (1995) *J. Biomol. NMR 6*, 277−293.
44. Braunschweiler, L., and Ernst, R. R. (1983) *J. Magn. Reson. 53*, 521−528.
45. Jeener, J., Meier, B. H., Bachmann, P., and Ernst, R. R. (1979) *J. Chem. Phys. 71*, 4546−4553.
46. Piotto, M., Saudek, V., and Sklenar, V. (1992) *J. Biomol. NMR 2*, 661−665.
47. Grzesiek, S., and Bax, A. (1993) *J. Am. Chem. Soc. 115*, 12593−12594.
48. Shaka, A. J., Barker, P. B., and Freeman, R. (1985) *J. Magn. Reson. 64*, 547−552.
49. Marion, D., Driscoll, P. C., Kay, L. E., Wingfield, P. T., Bax, A., Gronenborn, A. M., and Clore, G. M. (1989) *Biochemistry 28*, 6150−6156.
50. Shaka, A. J., Lee, C. J., and Pines, A. (1988) *J. Magn. Reson. 77*, 274−293.
51. Rucker, S. P., and Shaka, A. J. (1989) *Mol. Phys. 68*, 509−517.
52. Vuister, G. W., Clore, G. M., Gronenborn, A. M., Powers, R., Garrett, D. S., Tschudin, R., and Bax, A. (1993) *J. Magn. Reson. B101*, 210.
53. Vuister, G. W., and Bax, A. (1993) *J. Am. Chem. Soc. 115*, 7772−7777.
54. Kuboniwa, H., Grzesiek, S., Delaglio, F., and Bax, A. (1994) *J. Biomol. NMR 4*, 871−878.
55. Shaka, A. J., Keeler, J., and Freeman, R. (1983) *J. Magn. Reson. 53*, 313−340.
56. Farrow, N. A., Muhandiram, R., Singer, A. U., Pascal, S. M., Kay, C. M., Gish, G., Shoelson, S. E., Pawson, T., Forman-Kay, J. D., and Kay, L. E. (1994) *Biochemistry 33*, 5984−6003.
57. Frenkiel, T., Bauer, C., Carr, M. D., Birdsall, B., and Feeney, J. (1990) *J. Magn. Reson. 90*, 420−425.
58. Wishart, D. S., Sykes, B. D., and Richards, F. M. (1991) *J. Mol. Biol. 222*, 311−333.
59. Wishart, D. S., Sykes, B. D., and Richards, F. M. (1992) *Biochemistry 31*, 1647−1651.
60. Wishart, D. S., and Sykes, B. D. (1994) *J. Biomol. NMR 4*, 171−180.
61. Wishart, D. S., Bigham, C. G., Holm, A., Hodges, R. S., and Sykes, B. D. (1995) *J. Biomol. NMR 5*, 67−81.
62. Merutka, G., Dyson, H. J., and Wright, P. E. (1995) *J. Biomol. NMR 5*, 14−24.
63. Viguera, A. R., Jimenez, M. A., Rico, M., and Serrano, L. (1996) *J. Mol. Biol. 255*, 507−521.
64. Braun, D., Wider, G., and Wuthrich, K. (1994) *J. Am. Chem. Soc. 116*, 8466−8469.
65. Wuthrich, K. (1986) *NMR of Proteins and Nucleic Acids*, Wiley, New York.
66. Waltho, J. P., Feher, V. A., Merutka, G., Dyson, H. J., and Wright, P. E. (1993) *Biochemistry 32*, 6337−6347.
67. Brant, D. A., Miller, W. G., and Flory, P. J. (1967) *J. Mol. Biol. 23*, 47−65.
68. Anderson, A. G., and Hermans, J. (1988) *Proteins: Struct., Funct., Genet. 3*, 262−265.
69. Smith, L. J., Bolin, K. A., Schwalbe, H., MacArthur, M. W., Thornton, J. M., and Dobson, C. M. (1996) *J. Mol. Biol. 255*, 494−506.
70. van Mierlo, C. P., Darby, N. J., Keeler, J., Neuhaus, D., and Creighton, T. E. (1993) *J. Mol. Biol. 229*, 1125−1146.
71. Alexandrescu, A. T., and Shortle, D. (1994) *J. Mol. Biol. 242*, 527−546.
72. Farrow, N. A., Zhang, O., Forman-Kay, J. D., and Kay, L. E. (1995) *Biochemistry 34*, 868−878.
73. Buck, M., Schwalbe, H., and Dobson, C. M. (1996) *J. Mol. Biol. 257*, 669−683.
74. Farrow, N. A., Zhang, O., Forman-Kay, J. D., and Kay, L. E. (1997) *Biochemistry 36*, 2390−2402.
75. Wrabl, J. O., and Shortle, D. (1996) *Protein Sci. 5*, 2343−2352.
76. Lipari, G., and Szabo, A. (1982) *J. Am. Chem. Soc. 104*, 4546−4559.
77. Lipari, G., and Szabo, A. (1982) *J. Am. Chem. Soc. 104*, 4559−4570.
78. Mandel, A. M., Akke, M., and Palmer, A. G., 3rd (1995) *J. Mol. Biol. 246*, 144−163.
79. Munoz, V., Thompson, P. A., Hofrichter, J., and Eaton, W. A. (1997) *Nature 390*, 196−199.
80. Nelson, J. W., and Kallenbach, N. R. (1986) *Proteins: Struct., Funct., Genet. 1*, 211−217.
81. Ponnuswamy, P. K. (1993) *Prog. Biophys. Mol. Biol. 59*, 57−103.
82. Williams, S., Causgrove, T. P., Gilmanshin, R., Fang, K. S., Callender, R. H., Woodruff, W. H., and Dyer, R. B. (1996) *Biochemistry 35*, 691−697.
83. Thompson, P. A., Eaton, W. A., and Hofrichter, J. (1997) *Biochemistry 36*, 9200−9210.
84. Wright, P. E., Dyson, H. J., and Lerner, R. A. (1988) *Biochemistry 27*, 7167−7175.
85. Dyson, H. J., Rance, M., Houghten, R. A., Lerner, R. A., and Wright, P. E. (1988) *J. Mol. Biol. 201*, 161−200.
86. Sheinerman, F. B., and Brooks, C. L., 3rd (1998) *Proc. Natl. Acad. Sci. U.S.A. 95*, 1562−1567.
87. Kraulis, P. J. (1991) *J. Appl. Crystallogr. 24*, 946−950.

BI9920230